High-efficiency B_4C/Mo_2C alternate multilayer grating for monochromators in the photon energy range from 07 to 34 keV

Fadi Choueikani, Bruno Lagarde, Franck Delmotte, Michael Krumrey, François Bridou, Muriel Thomasset, Evgueni Meltchakov, François Polack

High-efficiency B_4C/Mo_2C alternate multilayer grating for monochromators in the photon energy range from 0.7 to 3.4 keV

Fadi Choueikani,[1,2,*] Bruno Lagarde,[2] Franck Delmotte,[1] Michael Krumrey,[3] Françoise Bridou,[1] Muriel Thomasset,[2] Evgueni Meltchakov,[1] and François Polack[2]

[1]*Laboratoire Charles Fabry, Institut d'Optique, CNRS, Univ Paris Sud, 2 avenue Augustin Fresnel, 91127 Palaiseau Cedex, France*

[2]*Synchrotron SOLEIL,L'Orme des Merisiers, Saint-Aubin, BP48, 91192 Gif-sur-Yvette, France*

[3]*Physikalisch-Technische Bundesanstalt (PTB),Abbestrasse 2-12, 10587 Berlin, Germany*

**Corresponding author: choueikani@synchrotron-soleil.fr*

Received January 31, 2014; revised March 1, 2014; accepted March 2, 2014;
posted March 3, 2014 (Doc. ID 205615); published March 31, 2014

An alternate multilayer (AML) grating has been prepared by coating an ion etched lamellar grating with a B_4C/Mo_2C multilayer (ML) having a layer thickness close to the groove depth. Such a structure behaves as a 2D synthetic crystal and can reach very high efficiencies when the Bragg condition is satisfied. This AML coated grating has been characterized at the SOLEIL Metrology and Tests Beamline between 0.7 and 1.7 keV and at the four-crystal monochromator beamline of Physikalisch-Technische Bundesanstalt (PTB) at BESSY II between 1.75 and 3.4 keV. A peak diffraction efficiency of nearly 27% was measured at 2.2 keV. The measured efficiencies are well reproduced by numerical simulations made with the electromagnetic propagation code CARPEM. Such AML gratings, paired with a matched ML mirror, constitute efficient monochromators for intermediate energy photons. They will extend the accessible energy for many applications as x-ray absorption spectroscopy or x-ray magnetic circular dichroism experiments.

OCIS codes: (230.4170) Multilayers; (340.6720) Synchrotron radiation; (260.6048) Soft x-rays; (340.7470) X-ray mirrors; (160.4760) Optical properties.
http://dx.doi.org/10.1364/OL.39.002141

The domain of synchrotron radiation features a transition in beamline technology between hard and soft x-rays. In the hard x-ray range, the energy selection is performed by Bragg reflection on single crystals. The accessible energy range is limited toward low energies by the unit cell size of available crystal and their stability under radiation (≈2 keV for Si, ≈1.75 keV for InSb) [1,2]. For soft x-rays, reflective gratings with lamellar, or more often, triangular (blazed) groove profiles are used under grazing incidence. Despite innovations in grating fabrication processes [3,4], the low efficiency of gratings still limits their use of energy above approximately 2.2 keV. Nevertheless, high-efficiency diffraction gratings are of prime importance for some applications in the energy range up to 3.5 keV. For example, x-ray absorption spectroscopy and x-ray magnetic circular dichroism experiments at *M*-edges of the rare earth elements and at the *K*-edge of sulfur would benefit from alternate multilayer (AML) gratings.

At lower energy ranges, in the domain of extreme ultraviolet, multilayer (ML)-coated lamellar gratings have been proposed as a way to enhance the efficiency [5,6]. Recently, ML-coated blazed gratings have been distinguished [7–9] with a reported diffraction efficiency approximately 44% at 13.1 nm (≈95 eV). In the soft x-rays domain, lamellar ML amplitude gratings have been described, but the reported efficiency was only around 8% at 1.5 keV [10,11]. Ways to improve the efficiency and selectivity of blazed grating in this spectral range were also shown [12,13]. However, producing a low blaze angle 1 deg or less as required is a difficult task. Additionally, maintaining the groove profile geometry on the large surface needed for implementation in a beamline monochromator is even more challenging. An alternative would be using an AML grating [14]. As shown in Fig. 1, the AML grating presents a double periodicity at nanometer scale. In the plane of the surface, the period is the pitch p of the laminar grating while it is the $2d$ spacing of the ML in the vertical direction. Therefore, an AML grating has properties similar to a crystal with the advantage of the freedom of choosing the periodicities.

In the ideal case depicted in Fig. 1, a perfect laminar profile is coated with a perfect ML and all the layers have a thickness equal to the grating groove depth. In the cross-section of the grating, the two materials of the ML alternate are in a checkerboard structure and the Bragg planes are defined by their angle with respect to the grating plane:

$$\theta_{(m,n)} = \tan^{-1}\left(\frac{2\,md}{np}\right), \tag{1}$$

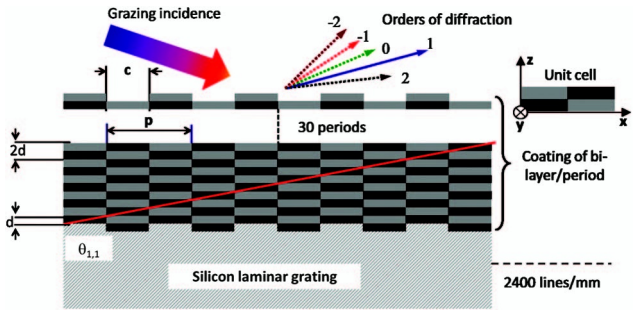

Fig. 1. Cross-section of a simple binary model of an ideal AML grating, realized on a lamellar grating of equal lands and grooves by deposition of an ML whose thickness of each material is equal to the grove depth d. Also indicated are the pitch p and the groove width c of the grating. The oblique straight line marks the orientation of the (1,1) Bragg plane. The unit cell of the ideal lattice is shown in the right inset.

where m and n are the Miller indices (respectively along z and x axes) of the diffraction orders in the reciprocal lattice. The AML grating should offer a high-efficiency for the first diffraction order and reject others orders. As for crystals, the diffraction efficiency of the different orders depends on the symmetry of the unit cell (see the inset of Fig. 1) and on the optical constants of the involved materials [15]. Thus, the performance of AML gratings relies on an agreement between the thicknesses of each stacked layer and the depth of etching, as well as on the refractive index of each material.

In a previous study of Mo/Si AML, simulations and measurements were performed and results showed an efficiency amounting to about 50% of the expectations [16]. The difference was attributed to the rather strong diffusion of Mo into Si [17,18], affecting the symmetry of the checkerboard structure that is critical for the high performance of the AML grating. The solution, which is widely discussed in ML literature and consists of using a B_4C layer as a barrier between Mo and Si [17,18], cannot be used due to the required symmetry.

The choice of B_4C and Mo_2C as materials for the AML grating was widely discussed and justified in our previous work [19]. Actually, the B_4C and Mo_2C couple offers a high contrast of refractive index. In addition, compared with other systems such as B_4C/Mo and Mo/Si, the B_4C/Mo_2C ML presents less interdiffusion and is well modeled by a symmetric structure without interfacial layers. Figure 2 presents a comparison of the efficiency versus the photon energy between three different configurations of AML gratings: a supposedly perfect B_4C/Mo system, a realistic tri-layer B_4C/IL/Mo coating where IL is the interfacial layer (1.2 nm of thickness) [19], and an alternative B_4C/Mo_2C system. The simulations were performed for a perfect rectangular profile (2400 lines/mm, $d = 2.5$ nm, duty cycle $\Gamma = c/p = 0.48$), with our electromagnetic propagation code CARPEM (CARPEM, Calcul de Réseaux par Propagation Electro-Magnétique) [20]. All curves in Fig. 2 show efficiencies higher than previously published ML grating structures [10,11]. Two configurations offer efficiencies close to the ideal perfect system: B_4C (2.5 nm)/IL(1.2 nm)/Mo(1.3 nm) and B_4C/Mo_2C AML systems. However, the presence of an IL formed at the expense of the deposited material makes the layer thicknesses difficult to control. A small variation of layer thicknesses affects the checkerboard symmetry of the unit cell. Thus, the B_4C/Mo_2C ML appears as a better choice to achieve the AML grating because it is without IL with a more simple fabrication process.

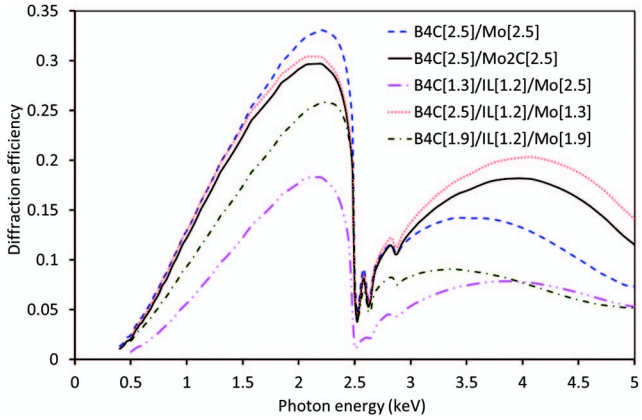

Fig. 2. CARPEM computations of diffraction efficiencies of the same lamellar 2400 lines/mm grating with a groove depth $d = 2.5$ nm, a duty cycle $\Gamma = c/p = 0.48$, coated with a 30 period ML, with materials and thicknesses (nm) as indicated in the graph legend.

An AML grating was fabricated by coating a B_4C/Mo_2C ML on a grating surface having a laminar groove profile. HORIBA Jobin Yvon fabricated this grating by ion-etching silicon substrate. The fabrication process does not affect the micro-roughness of the high polished substrate. Thanks to an absolute calibration given by a calibration transfer from the standard AFM of the Laboratoire National de Métrologie et d'Essais [21] to the atomic force microscopy (AFM) of Synchrotron SOLEIL, the accuracy of the measurements of the height of the grating was better than ±0.1 nm. Table 1 summarizes the features of the laminar grating substrate. It shows that the laminar grating actually presents a trapeze shaped profile which, due the very shallow height, is characterized by a slope around 4 deg, which actually corresponds to an inclined area of only 17%.

A magnetron sputtering deposition system described in [19,22] was used to deposit the B_4C/Mo_2C ML on the silicon laminar grating. Before the sputtering process, the chamber of preparation was pumped down to a base pressure of 7×10^{-8} mbar. The sputtering was performed at an argon gas pressure of 2×10^{-3} mbar. The targets size was 200 mm × 80 mm^2. The radio-frequency power was 150 W for the B_4C target and the direct current for the Mo_2C target was 0.07 A. The deposition rate was carefully calibrated using Cu-K_α grazing incidence reflectometry. It gives a good control on the achieved period with respect to the target value. In our case of the 2400 lines/mm grating, the groove depth was measured to be 2.51 nm and the target period was fixed to ≈5.0 nm. The duty cycle Γ was measured over the surface to vary between 0.44 and 0.48, slightly below the optimum value of 0.5 (for more details see Table 1). After the fabrication, a grazing incidence reflectometry was performed with the incidence plane parallel to the grating lines to avoid diffraction. We obtained 2.72 and 2.64 nm for the respective Mo_2C and B_4C thicknesses, hence a period of 5.36 nm.

The diffraction efficiency of this AML grating was measured at the low energy branch of the Metrology and Tests Beamline at Synchrotron SOLEIL [23] in the energy range from 0.7 to 1.7 keV, and at the four-crystal monochromateur (FCM) beamline of Physikalisch-

Table 1. AFM Measurements Performed on Lamellar Grating Used as Substrate[a]

Average Depth (nm)			Duty Cycle Γ (nm)			Angle (deg)		
L	C	R	L	C	R	L	C	R
2.42	2.51	2.51	0.45	0.48	0.44	4	4	5

[a]L, C, and R refer the left, center, and right of the grating surface. c/p is the duty cycle. The accuracy of measurements was better than ±0.1 nm.

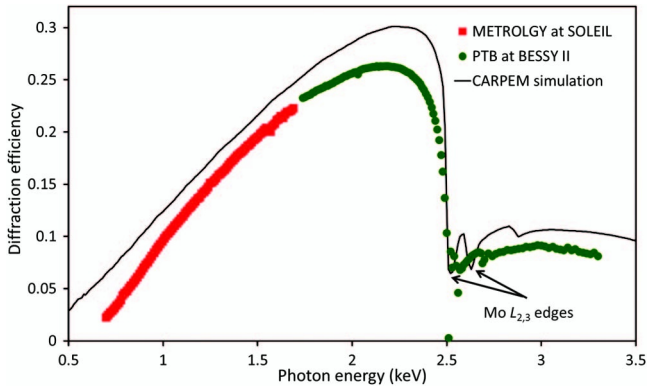

Fig. 3. Measured and calculated (with a rectangular profile) efficiency of the first diffraction order versus the photon energy in the range from 0.7 to 3.4 keV for a grating rotation angle $\Omega = 0.692$ deg and a duty cycle $\Gamma = 0.48$.

Technische Bundesanstalt (PTB) at BESSY II in the energy range from 1.75 to 3.4 keV [24]. The results are depicted in Figs. 3 and 4. In Fig. 3, the experimental efficiency of the first diffraction order versus the photon energy confirms the ability to obtain a high-efficiency ($\geq$10%) throughout a wide energy range (from 1 to 3.4 keV) by keeping a constant grating rotation angle $\Omega = 0.692$ deg. The angle Ω is defined as the grating rotation from specular reflection and is related to the grazing incidence and exit angles α and β by $\Omega = (\alpha - \beta)/2$. The fixed Ω value is an easy condition to drive a monochromateur using an AML grating very close to the Bragg condition. Figure 3 also shows a high-efficiency around 27% at 2.2 keV. The abrupt drop of the efficiency curve at 2.5 keV is due to the L_3 absorption edge of Mo. In addition, the agreement between the behavior of the experiment curves and the simulation result of CARPEM can be noted.

Figure 4 shows a detector scan at a fixed energy of 2.2 keV and at a fixed incidence angle of 7.8 deg. It illustrates the preferential coupling of almost all the incident flux into the first diffraction order when the Bragg condition is satisfied, which is a signature of 2D diffraction and explains why AML gratings can have very large efficiencies.

In Fig. 5, the measured reflectance of the first diffraction order at 2.2 keV is compared to a CARPEM

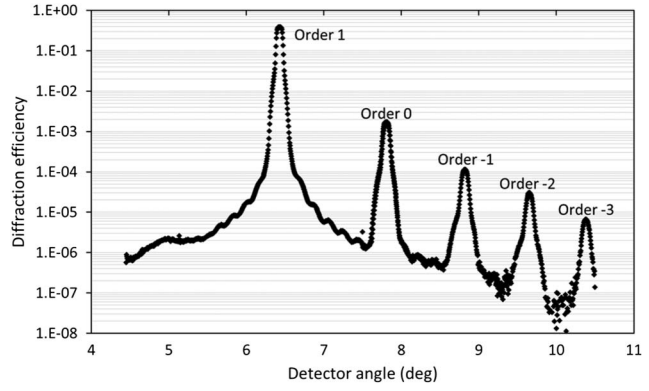

Fig. 4. Detector scan measured at the PTB FCM beamline for a constant incidence of 7.8 deg, a fixed energy of 2.2 keV and Ω of 0.692 deg satisfying the Bragg condition.

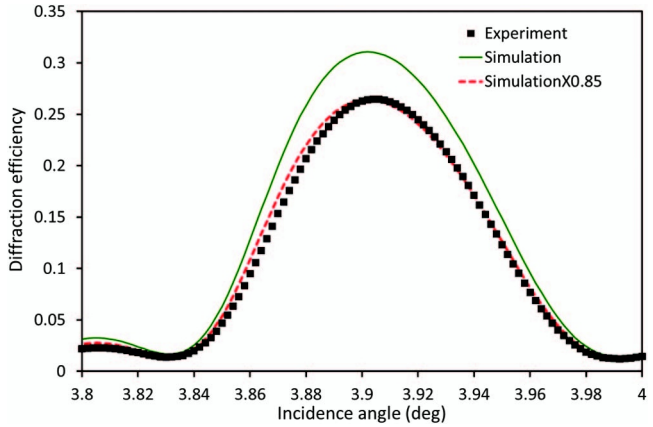

Fig. 5. Reflectivity profile of the first diffraction order at 2.2 keV. The values measured at PTB FCM beamline are compared to CARPEM simulations with the same parameters as in Fig. 3.

fit assuming a perfect rectangular profile of the grooves and a perfect replication of this profile by the deposited ML. In the fitting process, the reflectance is most sensitive to the respective thickness of Mo_2C and B_4C. Small changes of thicknesses result in a shift of the angle of maximum reflectivity. The obtained thicknesses agree with grazing Cu-K_α measurements to better than 0.1%. The width of the profile depends on the number of layer periods. An almost perfect agreement is found for 30 periods. The grating duty cycle Γ affects the peak efficiency. The best agreement was obtained for $\Gamma = 0.45$. The measured peak reflectance amounts to around 85% of the calculated maximum. The comparison confirms the good agreement between the measured efficiency and the best-fit simulations, as shown on Fig. 3. The difference between experiment and simulation can be explained by the rectangular profile assumption in the simulation, while the real profile is trapezoidal. In addition, the other imperfections of the structure, such as the interdiffusion and the interfacial roughness in the range of 0.1 nm, can contribute to reducing the efficiency from the computed 31% with $c/p = 0.45$ to the measured $\approx$27%. Unfortunately, the grating imperfections concerning geometry or roughness cannot be modeled by the CARPEM code in its present development stage.

We showed here the design realization and characterization of a B_4C/Mo_2C AML grating with a high-efficiency between 1 and 3.4 keV. Good agreement between calculated and measured performance was achieved. This AML grating, paired with a ML mirror of the same deviation, has been successfully installed into the DEIMOS beamline monochromator [25]. We are currently studying other ML material combinations in order to extend the high-efficiency of such monochromator at energy up to 5 keV.

This work is supported by a grant from the RTRA (réseaux thématiques de recherche avancée) program "Triangle de la Physique." The deposition and the characterization of the multilayers were performed on CEMOX (Centrale d'Elaboration et de Métrologie d'Optique X), a platform of the LUMAT federation (CNRS FR2764). The authors thank Stefanie Marggraf and Levent Cibik for their help during the experiments at

FCM beamline of PTB at BESSY II. The authors also thank Pascal Mercere for his help during the experiments at Metrology and Tests Beamline at Synchrotron SOLEIL. The authors acknowledge the remarkable work achieved by Audrey Liard and her team at HORIBA Jobin Yvon in preparing the ion etched grating substrate.

References

1. T. M. Mooney, T. Toellner, W. Sturhahn, E. E. Alp, and S. D. Shastri, Nucl. Instrum. Methods Phys. Res., Sect. A **347**, 348 (1994).
2. Y. V. Shvyd'ko, S. Stoupin, A. Cunsolo, A. H. Said, and X. Huang, Nat. Phys. **6**, 196 (2010).
3. D. Cocco, A. Bianco, B. Kaulich, F. Schaefers, M. Mertin, G. Reichardt, B. Nelles, and K. F. Heidemann, AIP Conf. Proc. **879**, 497 (2007).
4. B. Lagarde, F. Sirotti, A. Taleb-Ibrahimi, C. Miron, and F. Polack, J. Phys. Conf. Ser. **425**, 152022 (2013).
5. J. F. Seely, M. P. Kowalski, R. G. Cruddace, K. F. Heidemann, U. Heinzmann, U. Kleineberg, K. Osterried, D. Menke, J. C. Rife, and W. R. Hunter, Appl. Opt. **36**, 8206 (1997).
6. M. P. Kowalski, R. G. Cruddace, J. F. Seely, J. C. Rife, K. F. Heidemann, U. Heinzmann, U. Kleineberg, K. Osterried, D. Menke, and W. R. Hunter, Appl. Opt. **22**, 834 (1997).
7. D. L. Voronov, M. Ahn, E. H. Anderson, R. Cambie, C. H. Chang, E. M. Gullikson, R. K. Heilmann, F. Salmassi, M. L. Schattenburg, T. Warwick, V. V. Yashchuk, L. Zipp, and H. A. Padmore, Opt. Lett. **2615**, 35 (2010).
8. D. L. Voronov, E. H. Anderson, R. Cambie, S. Cabrini, S. D. Dhuey, L. I. Goray, E. M. Gullikson, F. Salmassi, T. Warwick, V. V. Yashchuk, and H. A. Padmore, Opt. Express **19**, 6320 (2011).
9. D. L. Voronov, E. H. Anderson, E. M. Gullikson, F. Salmassi, T. Warwick, V. V. Yashchuk, and H. A. Padmore, Opt. Lett. **37**, 1628 (2012).
10. R. Benbalagh, J.-M. André, R. Barchewitz, Ph. Jonnard, G. Julié, L. Mollard, G. Rolland, C. Remond, Ph. Troussel, R. Marmoret, and E. O. Filatova, Nucl. Instrum. Methods Phys. Res. A **541**, 590 (2005).
11. R. Benbalagh, J.-M. André, R. Barchewitz, M.-F. Ravet, A. Raynal, F. Delmotte, F. Bridou, G. Julié, A. Bosseboeuf, and Ph. Troussel, Nucl. Instrum. Methods Phys. Res. A **458**, 650 (2001).
12. A. Bianco, G. Sostero, B. Nelles, K. F. Heidemann, and D. Cocco, Proc. SPIE **5918**, 591810 (2005).
13. D. L. Voronov, S. Diez, P. Lum, S. A. Hidalgo, T. Warwick, N. A. Artemiev, and H. A. Padmore, Proc. SPIE **8848**, 88480Q (2013).
14. F. Polack, M. Idir, E. Jourdain, and A. Liard-Cloup, "Two-dimensional diffraction network with alternating multilayer stacks and method for the production thereof and spectroscopic devices comprising said networks," European patent application EP1700141 (July 17, 2005).
15. F. Polack, B. Lagarde, M. Idir, A. Liard Cloup, and E. Jourdain, AIP Conf. Proc. **879**, 639 (2007).
16. F. Polack, B. Lagarde, M. Idir, A. Liard-Cloup, E. Jourdain, and M. Roulliay, AIP Conf. Proc. **879**, 489 (2007).
17. A. Patteli, J. Ravagnana, V. Rigatoa, G. Salmasoa, D. Silvestrinia, E. Bontempic, and L. E. Deperoc, Appl. Surf. Sci. **238**, 262 (2004).
18. H. Maury, P. Jonnard, J.-M. André, J. Gautier, M. Roulliay, F. Bridou, F. Delmotte, M.-F. Ravet-Krill, A. Jérome, and P. Holliger, Thin Solid Films **514**, 278 (2006).
19. F. Choueikani, F. Bridou, B. Lagarde, E. Meltchakov, F. Polack, P. Mercere, and F. Delmotte, Appl. Phys. A **111**, 191 (2013).
20. A. Mirone, E. Delcamp, M. Idir, G. Cauchon, F. Polack, P. Dhez, and C. Bizeuil, Appl. Opt. **37**, 5816 (1998).
21. S. Ducourtieux and B. Poyet, Meas. Sci. Technol. **22**, 094010 (2011).
22. J. Gautier, F. Delmotte, F. Bridou, M. F. Ravet, F. Varniere, M. Rouilliay, A. Jerome, and I. Vickridge, Appl. Phys. A **88**, 719 (2007).
23. M. Idir, P. Mercere, T. Moreno, A. Delmotte, P. Da Silva, and M. H. Modi, AIP Conf. Proc. **1234**, 485 (2009).
24. M. Krumrey and G. Ulm, Nucl. Instrum. Methods Phys. Res. A **467-468**, 1175 (2001).
25. P. Ohresser, E. Otero, F. Choueikani, K. Chen, S. Stanescu, F. Deschamps, T. Moreno, F. Polack, B. Lagarde, J.-P. Daguerre, F. Marteau, F. Scheurer, L. Joly, J. P. Kappler, and B. Mulle, Rev. Sci. Instrum. **85**, 013106 (2014).